J Nanopart Res (2015) 17:82
DOI 10.1007/s11051-015-2891-y

RESEARCH PAPER

Core–shell monodisperse spherical $mSiO_2$/Gd_2O_3:Eu^{3+}@$mSiO_2$ particles as potential multifunctional theranostic agents

Daniil A. Eurov · Dmitry A. Kurdyukov · Demid A. Kirilenko · Julia A. Kukushkina · Alexei V. Nashchekin · Alexander N. Smirnov · Valery G. Golubev

Received: 17 July 2014 / Accepted: 27 January 2015

Abstract Core–shell nanoparticles with diameters in the range 100–500 nm have been synthesized as monodisperse spherical mesoporous (pore diameter 3 nm) silica particles with size deviation of less than 4 %, filled with gadolinium and europium oxides and coated with a mesoporous silica shell. It is shown that the melt technique developed for filling with gadolinium and europium oxides provides a nearly maximum filling of mesopores in a single-run impregnation, with gadolinium and europium uniformly distributed within the particles and forming no bulk oxides on their surface. The coating with a shell does not impair the monodispersity and causes no coagulation. The coating technique enables controlled variation of the shell thickness within the range 5–100 % relative to the core diameter. The thus produced nanoparticles are easily dispersed in water, have large specific surface area (300 m^2 g^{-1}) and pore volume (0.3 cm^3 g^{-1}), and are bright solid phosphor with superior stability in aqueous media. The core–shell structured particles can be potentially used for cancer treatment as a therapeutic agent (gadolinium neutron-capture therapy and drug delivery system) and, simultaneously, as a multimodal diagnostic tool (fluorescence and magnetic resonance imaging), thereby serving as a multifunctional theranostic agent.

Keywords Core–shell nanoparticles · Mesoporous silica · Theranostic agent · Gadolinium · Europium

Electronic supplementary material The online version of this article (doi:10.1007/s11051-015-2891-y) contains supplementary material, which is available to authorized users.

D. A. Eurov (✉) · D. A. Kurdyukov · D. A. Kirilenko · J. A. Kukushkina · A. V. Nashchekin · A. N. Smirnov · V. G. Golubev
Ioffe Physical–Technical Institute, 194021 St. Petersburg, Russia
e-mail: edan@mail.ru

D. A. Kurdyukov
ITMO University, 197101 St. Petersburg, Russia

Introduction

One of the most important tasks of modern medicine is to combine the therapeutic and diagnostic functions within a single formulation to raise the curing efficiency, reduce the off-target toxicity, and on the whole improve the results of curing and quality of life of oncology patients (Lammers et al. 2012; Cheng et al. 2012; Kim et al. 2013). Such formulations have been named theranostic agents. In contrast to vehicles for delivery of, separately, imaging agents and drugs, theranostic agents are capable of simultaneously delivering biomarkers and therapeutics to specific sites or organs and thereby enable diagnostics and disease therapy in a single procedure. Combination of diagnostic and therapeutic means in a single formulation makes it possible to obtain information about

Published online: 08 February 2015

the localization of a drug and a pathological process, which enables substantiated decisions about the choice, dosage, and timing of application of a drug and about curing strategies. Nanoparticles of interest for theranostics have been produced from various materials (Peer et al. 2007; Shi 2009; Minelli et al. 2010; Behrens 2011; Barreto et al. 2011).

A particular place among the materials that are promising for theranostics is occupied by mesoporous silica ($mSiO_2$) nanoparticles (Slowing et al. 2007; Vivero-Escoto et al. 2010; Taylor-Pashow et al. 2010; Rosenholm et al. 2010; Wu et al. 2011; Ambrogio et al. 2011; Tang et al. 2012; Colilla et al. 2013). These nanoparticles possess unique structural characteristics: large specific surface area (>700 $m^2\ g^{-1}$) and pore volume (>1 $cm^3\ g^{-1}$), variable average pore diameter (2–10 nm), chemically stable mesostructure, two functional surfaces (exterior surface of particles and interior surface of pores), and controllable particle shape and size. Owing to the unique mesoporous structure and large specific surface area, particles of this kind, used as containers, have a high capacity for accumulation of various molecules. The ordered structure of pores with variable size and configuration enables a homogenous incorporation of guest molecules with different sizes and properties. $mSiO_2$ particles can protect pharmaceutical cargoes, such as drugs, imaging agents, enzymes, and oligonucleotides, from premature release and undesirable degradation in harsh media before reaching the target.

In this study, we synthesized monodisperse spherical $mSiO_2$ particles filled with amorphous gadolinium and europium oxides ($mSiO_2/Gd_2O_3:Eu^{3+}$) and coated with a mesoporous silica shell ($mSiO_2/Gd_2O_3:Eu^{3+}@mSiO_2$). The particles are a promising material for development of a multifunctional system for theranostics of tumor diseases. Figure 1 shows schematically the functional capacity of the synthesized nanocomposite $mSiO_2/Gd_2O_3:Eu^{3+}@mSiO_2$ particles. Encapsulation of $Gd_2O_3:Eu^{3+}$ in $mSiO_2$ particles enables their use in tumor diagnostics by contrast-enhanced magnetic-resonance imaging (MRI) (Bruckman et al. 2013; Liu et al. 2012; Lin et al. 2004) and neutron-capture therapy of tumors (Geninatti-Crich et al. 2011; Leinweber et al. 2006; Kondrashina 2013; Hosmane et al. 2012). Owing to the presence of europium ions, the particles can be used in spectroscopic diagnostics as solid-state luminescent biomarkers [$Gd_2O_3:Eu^{3+}$ is one of the brightest

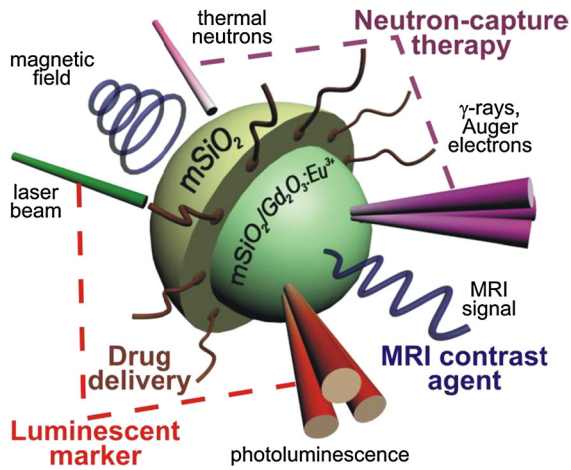

Fig. 1 Pictorial representation of the functionality of $mSiO_2/Gd_2O_3:Eu^{3+}@mSiO_2$ nanoparticles

phosphors (Di et al. 2011; Xu et al. 2011a, b)]. The synthetic route also allows one to infiltrate other hosts for Eu^{3+} ions i.e., Y_2O_3 (Cannas et al. 2003). The mesoporous shell enables application of the core–shell particles as containers for toxic chemotherapeutics.

The technique developed for production of $mSiO_2/Gd_2O_3:Eu^{3+}@mSiO_2$ particles enables a controlled variation of their diameter within the range 100–500 nm. The particles are spherical and the standard deviation σ of their size does not exceed 4 %, thanks to which they have identical hydrodynamic properties. In the future, with $mSiO_2/Gd_2O_3:Eu^{3+}@mSiO_2$ particles used as targeted drug delivery systems, this circumstance will make it possible to control the time in which particles penetrate into a tumor and that in which the pharmaceutical cargo is released. The presence of a system of cylindrical channels in the mesoporous shell, which have the same size and volume for each particle, will enable a precision control over the dosage of a toxic chemotherapeutic drug.

The method developed for introduction of gadolinium and europium oxides from melts of Gd(III) and Eu(III) nitrates into $mSiO_2$ pores by capillary impregnation of particles makes it possible to obtain in a single impregnation run a nearly maximum filling of the whole accessible pore volume and to preclude formation of a bulk oxide on the particle surface. The $Gd_2O_3:Eu^{3+}$ content of each particle is the same because of the nearly full filling of pores. This enables control over the dosage of the active substance when

the multifunctional particles we obtained are used in neutron-capture therapy and MRI diagnostics. In addition, Gd_2O_3:Eu^{3+} has an extremely low solubility in water, which provides its high biocompatibility (it will remain within the particles in aqueous media).

Thus, the synthesized multifunctional monodisperse $mSiO_2$/Gd_2O_3:Eu^{3+}@$mSiO_2$ particles can be potentially used as theranostic agents that simultaneously serve for four purposes: spectroscopic diagnostics, MRI diagnostics, chemotherapy, and neutron-capture therapy of cancer. When necessary, it is possible to use any required set of functions or all the four at once.

Experimental section

Materials

We used the following reagents: cetyltrimethylammonium bromide (CTAB, $C_{16}H_{33}N(CH_3)_3Br$), 99.99 %; aqueous ammonia (NH_3), 24 wt%; ethanol (C_2H_5OH), 95.7 vol%; deionized water (H_2O) with a resistance of 10 Ω; tetraethoxysilane (TEOS, $Si(OC_2H_5)_4$), 99.9 %; gadolinium oxide (Gd_2O_3), 99.99 %; europium oxide (Eu_2O_3), 99.99 %; and nitric acid (HNO_3), 70 wt%.

Synthesis of monodisperse $mSiO_2$ particles

Monodisperse spherical $mSiO_2$ particles were synthesized by hydrolysis of TEOS in a water–ethanol–ammonia medium containing cylindrical micelles of a surfactant structuring agent, CTAB. The NH_3–H_2O–C_2H_5OH–surfactant reaction mixture was prepared under vigorous stirring for 10 min. Then TEOS was poured into the mixture. The molar ratio of the reagents TEOS:NH_3:H_2O:C_2H_5OH:CTAB was 1:19:370:230:0.2. The synthesis duration was 1 h. The particles obtained were centrifuged, dried in air at 80 °C for 24 h, and calcined at 550 °C for 5 h.

Synthesis of nanocomposite $mSiO_2$/Gd_2O_3:Eu^{3+} particles

Eu^{3+}-doped Gd_2O_3 was synthesized within mesopores of the $mSiO_2$ particles via capillary impregnation with the melts of Gd(III) and Eu(III) nitrates and their subsequent decomposition. Gd_2O_3 (3 mmol) and Eu_2O_3 (0.15 mmol) were dissolved in HNO_3 and deionized water to obtain a 0.5 M nitrate solution. The solution pH was brought to five by addition of a necessary amount of aqueous ammonia. The resulting solution was evaporated at a temperature of 100 °C for 2 h. This yielded a melt of crystal hydrates of Gd(III) and Eu(III) nitrates. A weighed portion (300 mg) of the synthesized $mSiO_2$ particles was added to the melt. Then its temperature was raised to 600 °C (with a 1 deg min^{-1} step) and the calcination process was held until full decomposition of the nitrates. The resulting $mSiO_2$ particles containing Gd_2O_3:Eu^{3+} were subsequently redispersed in deionized water under ultrasonic agitation.

Synthesis of core–shell $mSiO_2$/Gd_2O_3:Eu^{3+}@$mSiO_2$ particles

The procedure used for coating of $mSiO_2$/Gd_2O_3:Eu^{3+} with an $mSiO_2$ shell is similar to that employed for synthesis of monodisperse $mSiO_2$ particles (Trofimova et al. 2013). As-prepared $mSiO_2$/Gd_2O_3:Eu^{3+} particles were dispersed in a mixed solution containing CTAB, deionized water, concentrated aqueous ammonia, and ethanol. TEOS was added dropwise under stirring to the resulting solution. After 6 h of further stirring, the particles obtained were centrifuged, dried, and calcined under the conditions specified in subsection that describes synthesis of monodisperse $mSiO_2$ particles.

Characterization

We measured EDX spectra and analyzed the morphology of the synthesized particles with a JEOL JSM-7001F scanning electron microscope. Transmission electron microscopy (TEM) measurements were made with JEOL JEM-2100F (equipped with Oxford Instruments INCA EDX spectrometer). Photoluminescence (PL) spectra were measured using a Horiba Jobin–Yvon T64000 spectrometer with an exciting light wavelength of 532 nm. The electrophoretic mobility of the particles was determined by the method of electrophoretic light scattering at a temperature of 25 °C with a Zetasizer Nano (Malvern, UK). The electrokinetic potential was calculated using the built-in software package of the analyzer. An adsorption-structural analysis was made with a Micromeritics ASAP 2020 analyzer at a temperature of 77 K, with nitrogen as the adsorbate. The specific surface area was calculated by the BET method, and

the pore size distribution was found using the nonlocal density functional theory, as it was done in the previous work (Trofimova et al. 2013). The true particle density was measured with a Micromeritics AccuPyc 1330 helium pycnometer (United States).

Results and discussion

In the first stage of the study, we synthesized monodisperse spherical $mSiO_2$ particles. The particles are formed in the course of synthesis via controlled coagulation of SiO_2–CTAB clusters, which provides their monodispersity (Trofimova et al. 2013). The synthesis procedure makes it possible to obtain spherical particles and to controllably vary their size in the range from 100 to 500 nm. Results for two diameters, 150 and 450 nm, are presented here. The particles have a spherical shape and the standard deviation of the particle sizes (for both diameters) does not exceed 4 %. The particles have an internal system of densely packed cylindrical pores 3.1 nm in diameter. The volume fraction of the pores is 50 % relative to the particle volume.

Scheme 1 shows how multifunctional nanocomposite monodisperse spherical $mSiO_2/Gd_2O_3:Eu^{3+}$@-$mSiO_2$ particles are synthesized. First, the as-grown monodisperse spherical $mSiO_2$ particles are impregnated with the melt of Gd(III) and Eu(III) nitrates, taken in a prescribed ratio. Then the particles are calcined in order to decompose the nitrates to oxides. This yields monodisperse spherical $mSiO_2$ particles filled with gadolinium and europium oxides ($mSiO_2/Gd_2O_3:Eu^{3+}$). The content of Eu in Gd_2O_3 was 5 mol%. X-ray analysis shows that the samples annealed at 600 °C are amorphous (Figure S1). Further, the synthesized particles are coated with an $mSiO_2$ shell. As already noted, the coating procedure is similar to that employed to synthesize the $mSiO_2$ particles (Trofimova et al. 2013).

Figure 2a shows a SEM image of the $mSiO_2/Gd_2O_3:Eu^{3+}$ particles obtained ($d = 450$ nm). It can be seen that, on being filled with the oxides, the particles remain spherical. A statistical processing of the SEM images of the $mSiO_2/Gd_2O_3:Eu^{3+}$ particles demonstrated that the standard deviation of their sizes does not exceed 4 %. This confirms that the procedure we developed to introduce $Gd_2O_3:Eu^{3+}$ into pores enables filling without changes in the shape and size of the as-grown particles.

The qualitative composition of the synthesized $mSiO_2/Gd_2O_3:Eu^{3+}$ particles was determined by energy-dispersive X-ray analysis (EDX). The particles were deposited onto a silicon substrate preliminarily covered with a 1-μm-thick layer of an iron-nickel alloy to exclude the possible contribution of the Si substrate in a quantitative analysis of the particle composition. The squares in the SEM image in Fig. 2a designate the regions in which the EDX spectra were measured. There is no Si-related peak in the EDX spectrum measured from the particle-free part of the substrate (region 1, Fig. 2a). This confirms that the iron–nickel layer does "shield" the silicon substrate and it makes no contribution in quantitative determination of Si in the particles.

Particles composed of Gd_2O_3 and SiO_2 have been obtained previously. In particular, the synthesis of $Gd_2O_3:RE^{3+}$ (RE = Eu, Er) luminescent particles coated with an $mSiO_2$ shell was described in (Xu et al. 2011a, b). The particles were produced by coating of spherical $Gd_{1-x}RE_x(OH)CO_3$ particles with a silica shell containing a surfactant and subsequent calcination. In this approach, it is difficult to control the size and shape of the resulting particles due to the substantial increase (by more than a factor of 3) in the density of Gd_2O_3, compared with the starting

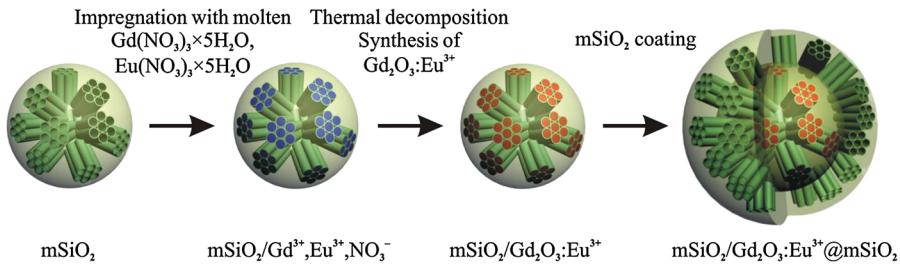

Scheme 1 General stages in synthesis of $mSiO_2/Gd_2O_3:Eu^{3+}$@$mSiO_2$ nanoparticles

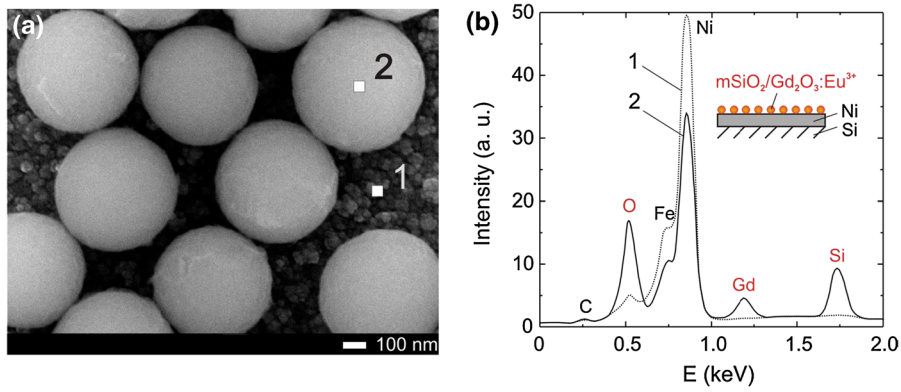

Fig. 2 **a** SEM image of $mSiO_2/Gd_2O_3:Eu^{3+}$ particles. The *white squares* indicate the regions in which EDX spectra were measured; **b** EDX spectra of the substrate (*1*) and a particle (*2*). Fe and Ni belong to the substrate

$Gd(OH)CO_3$, and to the evolution of a large amount of gases in the course of calcination.

In our study, we suggested to obtain $mSiO_2/Gd_2O_3:Eu^{3+}$ particles on the basis of a certainly monodisperse mesoporous template by introduction of $Gd_2O_3:Eu^{3+}$ into mesopores. The most frequently employed and the simplest method for introduction of various substances into porous materials is their capillary impregnation with solutions of the corresponding salts (Davydov et al. 2000; Grudinkin et al. 2008). A disadvantage of this technique is in the small degree of pore filling by a substance in a single impregnation run because not only the solute ions, but also solvent molecules find their way into the pores. As a result, the degree of pore filling by the substance in a single run is only several percent and dozens of impregnation runs are to be performed to achieve the maximum filling.

In this study, we suggested to introduce $Gd_2O_3:Eu^{3+}$ from melts. This approach made it possible to achieve a nearly maximum pore filling in a single impregnation run because, first, the melt contains a substantially larger amount of the needed substance as compared with the solution and, second, the filling is performed so the capillary impregnation of pores continues during the melt decomposition (de Jongh and Eggenhuisen 2013).

The content of Gd_2O_3 in $mSiO_2/Gd_2O_3:Eu^{3+}$ particles was determined by two methods: quantitative EDX analysis and pycnometry. According to the results of the quantitative EDX analysis, the fraction of Gd_2O_3 in the particles was 43 vol%. The pycnometric method was used to measure the true density of $mSiO_2/Gd_2O_3:Eu^{3+}$ particles, which was found to be 4.63 g/cm^3. Using this value of the true density, we calculated the fraction of Gd_2O_3 in the particles to be 47 vol%. (The Gd_2O_3 and SiO_2 densities were taken to be 7.41 and 2.1 g/cm^3, respectively.) The values obtained by two methods are in good agreement. Thus, because the fraction of pores in the as-grown monodisperse spherical $mSiO_2$ particles is 50 vol%, the procedure developed for introducing Gd and Eu oxides from salt melts enabled a nearly complete pore filling in a single run.

Figure 3 shows TEM images of $mSiO_2/Gd_2O_3:Eu^{3+}$ particles ($d = 450$ nm), which confirm that, on being filled with $Gd_2O_3:Eu^{3+}$, $mSiO_2$ particles remain spherical. A magnified image of a particle (Fig. 3b) shows the surface roughness due to the cluster structure of the material (Trofimova et al. 2013). It can be seen in Fig. 3b that gadolinium oxide doped with europium ions is localized within the particles and forms no bulk $Gd_2O_3:Eu^{3+}$ on the particle surface. If the bulk gadolinium oxide was present on the particle surface, the corresponding regions in the TEM image would be markedly darker than the rest of the particle because the heavy element Gd has a larger electron absorption coefficient than Si. The fact that the particles in the image are whole-colored is indicative of a homogeneous distribution of the oxides within pores of $mSiO_2$ particles. This is also confirmed by EDX maps of O (Kα1), Si (Kα1), and Gd (Lα1) for $mSiO_2/Gd_2O_3:Eu^{3+}$ particles (Fig. 3c).

Gadolinium oxide is not formed on the surface of $mSiO_2$ particles because the process of Gd(III) nitrate decomposition occurs directly within silica mesopores, rather than in the space between the $mSiO_2$ particles. The $Gd(NO_3)_3{\cdot}5H_2O$ melt wets the surface of hydrated $mSiO_2$. The wetting fluid fills mesopores and the space between the particles under the action of

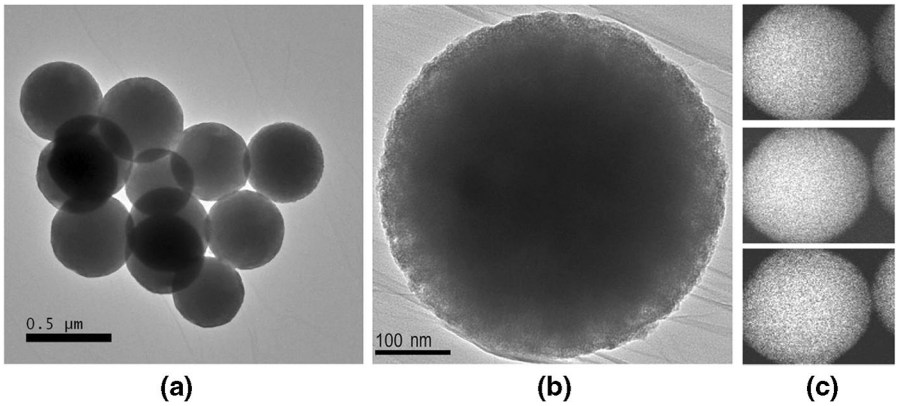

Fig. 3 **a** TEM image of $mSiO_2/Gd_2O_3:Eu^{3+}$ particles; **b** magnified TEM image of a single particle; **c** EDX maps of (from *top downward*) O (Kα1), Si (Kα1), Gd (Lα1), *circular* regions are of the same size equal to the sphere diameter

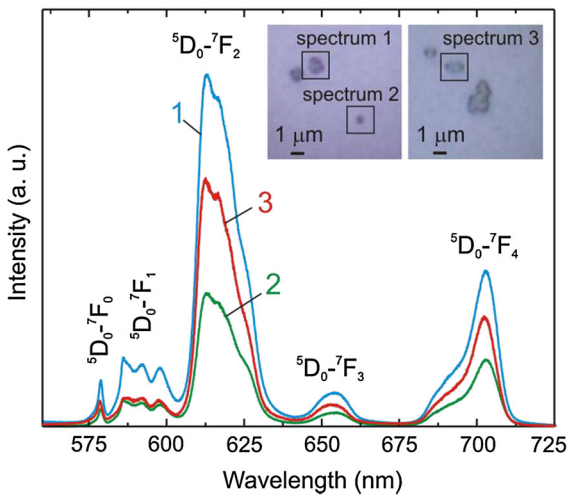

Fig. 4 PL spectra of $mSiO_2/Gd_2O_3:Eu^{3+}$ particles with different diameters upon excitation at 532 nm with a Nd:YAG laser: *1* 450 nm (group of particles); *2* 450 nm (single particle); *3* 150 nm (group of particles)

the capillary pressure, which is inversely proportional to the pore diameter according to Laplace's law. The distance between $mSiO_2$ particles exceeds by at least an order of magnitude the diameter of mesopores (3.1 nm). Consequently, the capillary pressure within the mesopores will also be ten times that between the particles. Therefore, the melt of Gd(III) nitrate crystal hydrate predominantly decomposes within mesopores, with the resulting gadolinium oxide mostly localized within the $mSiO_2$ particles.

Figure 4 shows PL spectra of $mSiO_2/Gd_2O_3:Eu^{3+}$ particles with diameters of 150 and 450 nm. The exciting light wavelength was 532 nm. Spectra 1 and 2 were measured for particles 450 nm in diameter from a group of particles and a single particle, respectively. Spectrum 3 was measured from a group of particles with a diameter of 150 nm. The insets in Fig. 4 show optical micrographs of the particles. It was impossible to measure a spectrum for a single 150-nm particle because this size is below the diffraction limit of the optical microscope. The PL spectra show a group of lines (Di et al. 2011; Xu et al. 2011a, b) associated with intracenter transitions in Eu^{3+} (the corresponding transitions are shown in the spectrum), with a clearly pronounced peak at a wavelength of 612 nm. The fact that the spectra are identical indicates that the composition and luminescent properties of each particle are the same. Prior to being analyzed by PL spectroscopy, the synthesized $mSiO_2/Gd_2O_3:Eu^{3+}$ particles were stored in an aqueous suspension for a week and after that were deposited on a silicon substrate and PL measurements were made. This evidences that the luminescent material we obtained is not susceptible to degradation in aqueous media.

The detailed site-selective and fluorescence line narrowing laser spectroscopy study of $mSiO_2/Gd_2O_3:Eu^{3+}$ particles is provided in (Feofilov et al. 2014). The selective excitation of the sample fluorescence definitively shows that Eu^{3+} ions are embedded in a highly disordered medium where the spectra are strongly inhomogeneously broadened as they are in glasses. It was concluded that the sample contains amorphous $Gd_2O_3:Eu^{3+}$ in the mesopores of $mSiO_2$ particles.

The measurements of the radiative lifetimes (τ_R) of the Eu^{3+} $^5D_0$ excited levels in the synthesized particles showed that τ_R varies from 1.4 to 1.7 ms depending on the size of the particles and their surrounding medium (Feofilov et al. 2014). These values are twice higher than those of the bulk. It evidences the amorphous nature of the environment of Eu^{3+} ions.

A study of the surface properties of $mSiO_2/Gd_2O_3:Eu^{3+}$ particles demonstrated that they have a surface charge different from that of as-grown $mSiO_2$. Figure 5 shows how the zeta potential depends on the pH of the medium for as-grown $mSiO_2$ particles and those filled with $Gd_2O_3:Eu^{3+}$. In the alkaline region, $mSiO_2/Gd_2O_3:Eu^{3+}$ particles have a lower (in absolute value) zeta potential than that for as-grown particles. In an alkaline medium, as-grown particles have a negative charge because of the dissociation of the SiO–H bond to give $Si–O^-$ on the surface. As the pH value becomes lower, the number of dissociated groups decreases, so that, in the end, the dissociation is completely suppressed in the acid medium, and just this behavior is observed in the plot (Fig. 5, curve 1). A presumable reason why $mSiO_2$ particles filled with $Gd_2O_3:Eu^{3+}$ are different is that gadolinium situated near the surface in particle pores behaves as a base by forming Gd–OH in the aqueous medium. This base does not dissociate in the alkaline medium; however, its presence on the particle surface makes lower the density of SiO–H groups. As a result, the negative charge of particles becomes smaller in absolute value, compared with the as-grown $mSiO_2$ particles (Fig. 5, curve 2). With decreasing pH, the dissociation of SiO–H becomes less pronounced. In the neutral region, Gd–OH starts to dissociate with elimination of the OH group and a positive charge is formed as a result. At pH $\sim$ 8, the negative charge on SiO^- is neutralized by the positive charge on $[–Gd–OH]^+$ or $[=Gd]^+$ surface groups and the surface charge of the particles becomes zero (the curve passes through the isoelectric point). At pH 6–7, a positive charge is observed on the particle surface (Fig. 5, curve 2). The further decrease of the charge with decreasing pH (in the acid region) is accounted for by the binding of $[–Gd–OH]^+$ or $[= Gd]^+$ surface groups with counter ions present in solution (in the case under consideration, with Cl– ions because the acid medium was created by addition of hydrochloric acid to the suspension of particles).

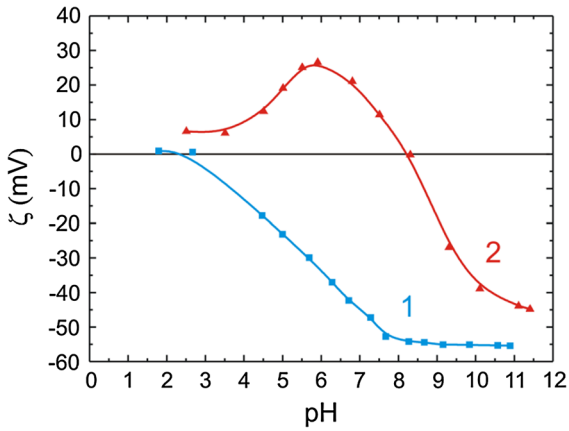

Fig. 5 Zeta potential versus pH curves for bare $mSiO_2$ particles (*1*) and $mSiO_2/Gd_2O_3:Eu^{3+}$ particles (*2*)

Figure 6 shows TEM images of $mSiO_2/Gd_2O_3:Eu^{3+}$ particles coated with an $mSiO_2$ shell in a single run (Fig. 6a, b) and in two runs (Fig. 6d, e). It can be seen that, on being coated with a shell, particles remain spherical and monodisperse ($\sigma < 4$ %) and do not coagulate. The coating of particles with a shell in several runs makes it possible to obtain, when necessary, a thicker shell. It is noteworthy that, when a thick shell is formed in a single run, it is necessary to use a larger amount of reagents. In particular, a higher concentration of the surfactant is required, which leads to coalescence of the particles. The coating of particles with a shell in several runs requires a lower concentration in each stage, which prevents the coalescence of the particles. The technique we developed makes it possible to obtain shells with a thickness of 5–100 % relative to the core diameter.

The particle core in the images is darker than the shell because the former contains Gd whose electron absorption coefficient is higher than that of Si, of which the particle shell is composed. The color images (Fig. 6c, f) are the composition maps of particles coated with a shell in one and two runs, respectively. It can be seen that $Gd_2O_3:Eu^{3+}$ is still homogeneously distributed within the core of $mSiO_2/Gd_2O_3:Eu^{3+}$@ $mSiO_2$ particles, and the shell is fully composed of SiO_2.

Figure 7 shows adsorption isotherms for as-grown $mSiO_2$ particles (d = 450 nm), $mSiO_2$ particles filled with gadolinium and europium oxides ($mSiO_2/Gd_2O_3:Eu^{3+}$), and $mSiO_2/Gd_2O_3:Eu^{3+}$ particles coated with a mesoporous shell in one and two runs. The as-grown $mSiO_2$ particles have large specific surface area (600 m^2 g^{-1}) and pore volume (0.50 cm^3 g^{-1}) and a

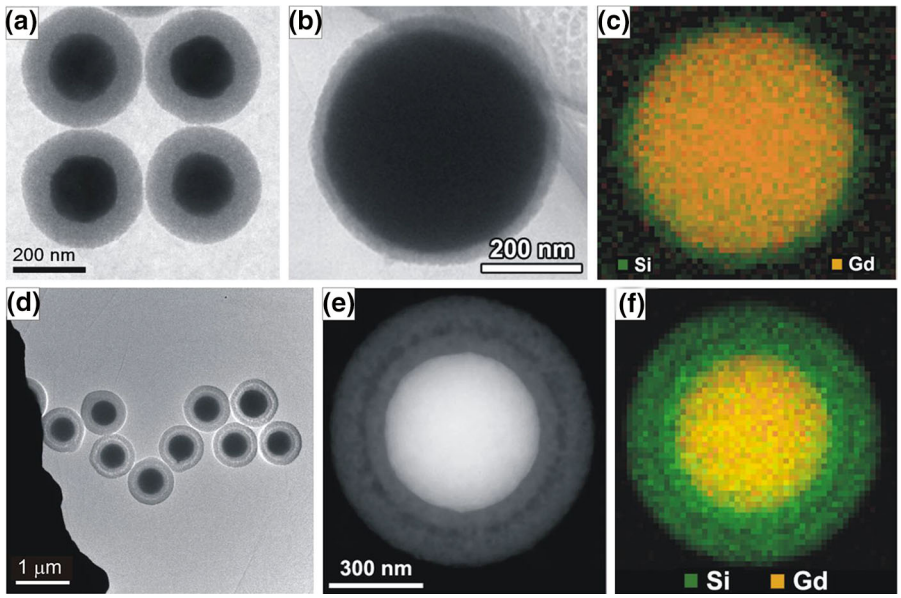

Fig. 6 TEM images of $mSiO_2/Gd_2O_3:Eu^{3+}$ particles coated with $mSiO_2$ ($mSiO_2/Gd_2O_3:Eu^{3+}@mSiO_2$). **a** 150 nm core, one-run coating (100 nm thickness); **b** 450 nm core, one-run coating (40 nm thickness); **d**, **e** 450 nm core, two-run coating (200 nm thickness); **c**, **f** EDX maps for one- and two-run coated 450 nm $mSiO_2/Gd_2O_3:Eu^{3+}@mSiO_2$ particles respectively

narrow pore size distribution (Fig. 7b, curve 1). The pore diameter is 3.10 ± 0.15 nm. After the particles are filled with the oxides (Fig. 7a, isotherm 2), a sharp decrease is observed in both the specific surface area (to 30 $m^2\ g^{-1}$) and pore volume (to 0.03 $cm^3\ g^{-1}$). The pores become fully closed (which indirectly confirms their nearly complete filling). Therefore, no pore size distribution is presented for these particles. After $mSiO_2/Gd_2O_3:Eu^{3+}$ particles were coated with a mesoporous silica shell in a single run (Fig. 7a, isotherm 3), their specific surface area and pore volume were 300 $m^2\ g^{-1}$ and 0.28 $cm^3\ g^{-1}$, respectively. However, a rather wide scatter of pore sizes is observed (Fig. 7b, curve 3), with a maximum at about 4 nm. The situation for particles shell-coated in two runs is similar (Fig. 7a, isotherm 4). The specific surface area and pore volume are 270 $m^2\ g^{-1}$ and 0.34 $cm^3\ g^{-1}$, respectively. Even though the pore size distribution is wide in this case (Fig. 7b, curve 4), there is a clearly pronounced maximum corresponding to a diameter of 3.1 nm, as for the as-grown $mSiO_2$ particles.

It is noteworthy that a narrow size distribution peaked at 3.1 nm is observed for nonporous spherical $mSiO_2$ particles with a mesoporous shell, as also for as-grown $mSiO_2$ particles (Figure S2). When $mSiO_2/Gd_2O_3:Eu^{3+}$ particles are coated with an $mSiO_2$ shell, the pH of the reaction mixture is ~9 and the surface charge of the particles is low (Fig. 5, curve 2). CTAB molecules in the vicinity of almost uncharged surface form the so-called platelet micelles (Raman et al. 1996), rather than cylindrical micelles produced in an ordinary synthesis when the surface of the particles is negatively charged (Trofimova et al. 2013). The overgrowth of these micelles with SiO_2 and the subsequent removal of organics yield pores of various diameters (substantially larger than 3.1 nm, which is the characteristic size of cylindrical pores) and just this circumstance is responsible for the broadening toward larger values in the pore size distribution plot (Fig. 7b, curve 3). The shell grows further via addition of SiO_2-coated aggregates of cylindrical CTAB micelles (Trofimova et al. 2013). It is this circumstance that is responsible for the appearance of a clearly pronounced characteristic maximum at 3.1 nm for particles coated with an $mSiO_2$ shell in two runs because the mesoporous shell synthesized in the first run "shields" the surface charge created by gadolinium. However, the general pore size distribution remains wide (Fig. 7b, curve 4) because all the available pores are taken into account in measurements.

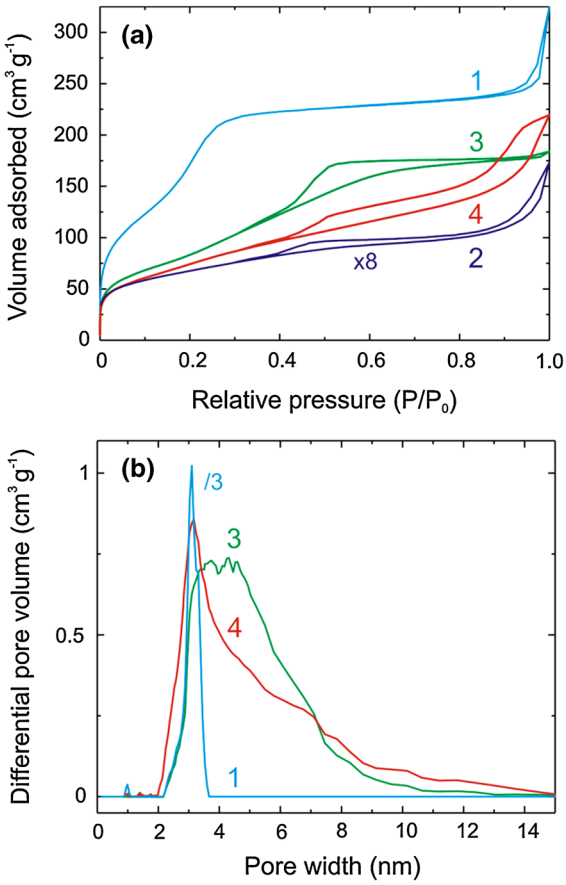

Fig. 7 **a** N_2 adsorption and desorption isotherms at 77 K for bare $mSiO_2$ particles (*1*), $mSiO_2/Gd_2O_3:Eu^{3+}$ particles (*2*), $mSiO_2/Gd_2O_3:Eu^{3+}@mSiO_2$ one-run coated (*3*), $mSiO_2/Gd_2O_3:Eu^{3+}@mSiO_2$ two-run coated (*4*); **b** pore size distribution for the same samples

Conclusion

Nanocomposite core–shell structured particles having the form of mesoporous silica particles filled with amorphous gadolinium and europium oxides and coated with a mesoporous silica shell were synthesized. The $mSiO_2/Gd_2O_3:Eu^{3+}@mSiO_2$ particles obtained in the study with sizes in the range 100–500 nm are spherical and highly monodisperse (the standard size deviation is smaller than 4 %). A procedure was developed for filling of as-grown monodisperse $mSiO_2$ particles with gadolinium and europium oxides via their capillary impregnation with melts of the corresponding nitrates. This procedure enables a nearly maximum pore filling in a single impregnation run. After the filling, $Gd_2O_3:Eu^{3+}$ is homogeneously distributed inside $mSiO_2$ particles, without forming a bulk oxide on their surface. The content of $Gd_2O_3:Eu^{3+}$ in $mSiO_2/Gd_2O_3:Eu^{3+}$ particles is about 45 vol% (at a pore fraction in as-grown $mSiO_2$ particles of 50 vol%). A procedure was developed for coating of $mSiO_2/Gd_2O_3:Eu^{3+}$ particles with an $mSiO_2$ shell. This procedure enables coating in both one and several runs, which makes it possible to raise the shell thickness without impairing the monodispersity of the particles or causing their coagulation. The thus obtained $mSiO_2/Gd_2O_3:Eu^{3+}@mSiO_2$ particles retain their spherical shape and the small standard size deviation (<4 %), and have large specific surface area (300 m^2 g^{-1}) and pore volume (0.3 cm^3 g^{-1}). The shell thickness can be controllably varied within the range 5–100 % relative to the core diameter. Oxides of Si, Gd, Eu constituting the particles are biocompatible. The core–shell structured nanoparticles show a bright luminescence and a superior stability in aqueous media. They can be potentially used for cancer treatment as a therapeutic agent (gadolinium neutron-capture therapy and drug delivery system) and, simultaneously, as a multimodal diagnostic tool (fluorescence and magnetic resonance imaging), thereby serving as a multifunctional theranostic agent.

Acknowledgments The authors are grateful to E. Yu. Stovpiaga for assistance in syntheses of monodisperse $mSiO_2$ particles, to V. V. Sokolov for measurements of the true density of the samples, to A. V. Shvidchenko for assistance in measurements of the zeta potential of the particles, and to V. Yu. Davydov and A. A. Sitnikova for fruitful discussions. This work was supported by the Russian Foundation for Basic Research (project no. 15-52-12011) and the Program no. 1 of the Presidium of the Russian Academy of Sciences. The study was in part carried out at the Joint Research Center "Material science and characterization in advanced technology".

References

Ambrogio MW, Thomas CR, Zhao Y-L, Zink JI, Stoddart JF (2011) Mechanized silica nanoparticles: a new frontier in theranostic nanomedicine. Acc Chem Res 44:903–913

Barreto JA, O'Malley W, Kubeil M, Graham B, Stephan H, Spiccia L (2011) Nanomaterials: applications in cancer imaging and therapy. Adv Mater 23:H18–H40

Behrens S (2011) Preparation of functional magnetic nanocomposites and hybrid materials: recent progress and future directions. Nanoscale 3:877–892

Bruckman MA, Yu X, Steinmetz NF (2013) Engineering Gd-loaded nanoparticles to enhance MRI sensitivity via T_1 shortening. Nanotechnology 24:462001

Cannas C, Casu M, Mainas M, Musinu A, Piccaluga G, Polizzi S, Speghinic A, Bettinelli M (2003) Synthesis, characterisation and optical properties of nanocrystalline Y_2O_3–Eu^{3+} dispersed in a silica matrix by a deposition–precipitation method. J Mater Chem 13:3079–3084

Cheng Z, Zaki AA, Hui JZ, Muzykantov VR, Tsourkas A (2012) Multifunctional nanoparticles: cost versus benefit of adding targeting and imaging capabilities. Science 338:903–910

Colilla M, González B, Vallet-Regí M (2013) Mesoporous silica nanoparticles for the design of smart delivery nanodevices. Biomater Sci 1:114–134

Davydov VYu, Golubev VG, Kartenko NF, Kurdyukov DA, Pevtsov AB, Sharenkova NV, Brogueira P, Schwarz R (2000) Fabrication and structural studies of opal-III nitride nanocomposites. Nanotechnology 11:291–294

de Jongh PE, Eggenhuisen TM (2013) Melt infiltration: an emerging technique for the preparation of novel functional nanostructured materials. Adv Mater 25:6672–6690

Di W, Ren X, Zhao H, Shirahata N, Sakka Y, Qin W (2011) Single-phased luminescent mesoporous nanoparticles for simultaneous cell imaging and anticancer drug delivery. Biomaterials 32:7226–7233

Feofilov SP, Kulinkin AB, Eurov DA, Kurdyukov DA, Golubev VG (2014) Fluorescence spectroscopy study of mesoporous SiO_2 particles containing Gd_2O_3:Eu^{3+}. Mater Res Express 1:025019

Geninatti-Crich S, Alberti D, Szabo I, Deagostino A, Toppino A, Barge A, Ballarini F, Bortolussi S, Bruschi P, Protti N, Stella S, Altieri S, Venturello P, Aime S (2011) MRI-guided neutron capture therapy by use of a dual gadolinium/boron agent targeted at tumour cells through upregulated low-density lipoprotein transporters. Chem Eur J 17:8479–8486

Grudinkin SA, Kaplan SF, Kartenko NF, Kurdyukov DA, Golubev VG (2008) Opal-hematite and opal-magnetite films: lateral infiltration, thermodynamically driven synthesis, photonic crystal properties. J Phys Chem C 112:17855–17861

Hosmane NS, Maguire JA, Zhu Y, Takagaki M (2012) Boron and gadolinium neutron capture therapy for cancer treatment. World scientific publishing company Co Pte Ltd, Singapore

Kim TH, Lee S, Chen X (2013) Nanotheranostics for personalized medicine. Expert Rev Mol Diagn 13:257–269

Kondrashina OV (2013) A targeted drug delivery system of Gd^{3+} for neutron capture therapy against cancer is metalorganic magnetic nanoparticles. J Nanomed Biother Discov 3:1000116

Lammers T, Rizzo LY, Storm G, Kiessling F (2012) Personalized nanomedicine. Clin Cancer Res 18:4889–4894

Leinweber G, Barry DP, Trbovich MJ, Burke JA, Drindak NJ, Knox HD, Ballad RV, Block RC, Danon Y, Severnyak LI (2006) Neutron capture and total cross-section measurements and resonance parameters of gadolinium. Nucl Sci Eng 154:261–279

Lin Y-S, Hung Y, Su J-K, Lee R, Chang C, Lin M-L, Mou C-Y (2004) Gadolinium(III)-incorporated nanosized mesoporous silica as potential magnetic resonance imaging contrast agents. J Phys Chem B 108:15608–15611

Liu Z, Liu X, Yuan Q, Dong K, Jiang L, Li Z, Ren J, Qu X (2012) Hybrid mesoporous gadolinium oxide nanorods: a platform for multimodal imaging and enhanced insoluble anticancer drug delivery with low systemic toxicity. J Mater Chem 22:14982–14990

Minelli C, Lowe SB, Stevens MM (2010) Engineering nanocomposite materials for cancer therapy. Small 6:2336–2357

Peer D, Karp JM, Hong S, Farokhzad OC, Margalit R, Langer R (2007) Nanocarriers as an emerging platform for cancer therapy. Nature Nanotech 2:751–760

Raman NK, Anderson MT, Brinker CJ (1996) Template-based approaches to the preparation of amorphous, nanoporous silicas. Chem Mater 8:1682–1701

Rosenholm JM, Sahlgren C, Lindén M (2010) Towards multifunctional, targeted drug delivery systems using mesoporous silica nanoparticles—opportunities & challenges. Nanoscale 2:1870–1883

Shi D (2009) Integrated multifunctional nanosystems for medical diagnosis and treatment. Adv Funct Mater 19:3356–3373

Slowing II, Trewyn BG, Giri S, Lin VS-Y (2007) Mesoporous silica nanoparticles for drug delivery and biosensing applications. Adv Funct Mater 17:1225–1236

Tang F, Li L, Chen D (2012) Mesoporous silica nanoparticles: synthesis, biocompatibility and drug delivery. Adv Mater 24:1504–1534

Taylor-Pashow KML, Rocca JD, Huxford RC, Lin W (2010) Hybrid nanomaterials for biomedical applications. Chem Commun 46:5832–5849

Trofimova EYu, Kurdyukov DA, Yakovlev SA, Kirilenko DA, Kukushkina YuA, Nashchekin AV, Sitnikova AA, Yagovkina MA, Golubev VG (2013) Monodisperse spherical mesoporous silica particles: fast synthesis procedure and fabrication of photonic-crystal films. Nanotechnology 24:155601

Vivero-Escoto JL, Slowing II, Trewyn BG, Lin VS-Y (2010) Mesoporous silica nanoparticles for intracellular controlled drug delivery. Small 6:1952–1967

Wu S-H, Hung Y, Mou C-Y (2011) Mesoporous silica nanoparticles as nanocarriers. Chem Commun 47:9972–9985

Xu Z, Gao Y, Huang S, P'an Ma, Lin J, Fang J (2011a) A luminescent and mesoporous core-shell structured Gd_2O_3:Eu^{3+}@nSiO_2@mSiO_2 nanocomposite as a drug carrier. Dalton Trans 40:4846–4854

Xu Z, Li C, P'an Ma, Hou Z, Yang D, Kang X, Lin J (2011b) Facile synthesis of an up-conversion luminescent and mesoporous Gd_2O_3:Er^{3+}@nSiO_2@mSiO_2 nanocomposite as a drug carrier. Nanoscale 3:661–667